# Modeling Gas Flow Dynamics in Metal−Organic Frameworks

Jiaolong Jiang,[†] Anna M. Plonka,[†] Anatoly I. Frenkel,*[,†,‡] and Dilip Gersappe*[,†]

[†]Department of Materials Science and Chemical Engineering, Stony Brook University, Stony Brook, New York 11794 United States
[‡]Division of Chemistry, Brookhaven National Laboratory, Upton, New York 11973 United States

Ⓢ *Supporting Information*

ABSTRACT: Modeling fluid flow dynamics in metal organic frameworks (MOFs) is a required step toward understanding mechanisms of their activity as novel catalysts, sensors, and filtration materials. We adapted a lattice Boltzmann model, previously used for studying flow dynamics in meso- and microporous media, to the nanoscale dimensions of the MOF pores. Using this model, rapid screening of permeability of a large number of MOF structures, in different crystallographic directions, is possible. The method was illustrated here on the example of an anisotropic MOF, for which we calculated permeability values in different flow directions. This method can be generalized to a large class of MOFs and used to design MOFs with the desired gas flow permeabilities.
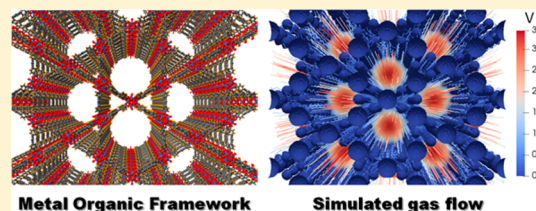
Metal organic frameworks (MOFs) are an emerging class of crystalline materials, consisting of inorganic cores connected by organic linkers to form extended networks with hierarchical nanoscale pores and ultrahigh surface areas.[1,2] These pore structures can be rigid or flexible, simple or interconnected, with varying pore apertures allowing for extraordinary tuning[3] for applications ranging from catalysis,[4,5] sensing,[6,7] and adsorption-based gas separation to size-determined gas separation through membranes.[8−12] For such applications as catalytic decontamination of chemical warfare agents, MOFs have attracted intense research due to the combination of their permeability and reactivity.[13−16] While molecular dynamics simulations of diffusive transport in MOFs have been reported before,[17,18] for many applications, such as in pressure gradient driven flows, the kinetics of adsorption and transport are coupled, and it is critical to develop theoretical models of the transport in MOF in the presence of a flow field. In all of these applications, the permeability of the MOF is key to its performance because it affects both the adsorption characteristics as well as the residence time distributions of the transported components.

Transport mechanisms in porous media fall between two limits: concentration-gradient-driven diffusion and pressure-gradient-driven flows. The interaction between an analyte and the medium can be considerably different depending on the mode of transport. Diffusional transport is controlled by random walk statistics, while pressure-gradient-driven transport is governed by the flow streamlines, which can advect the analyte through the medium. Modeling these streamlines, however, cannot be done by models developed for diffusional transport, such as molecular dynamics (MD), particularly at experimentally valid flow rates due to their small time steps, nor can they be done by using coarse-grained resistive networks that have been developed to determine permeability in nanoporous systems.[19] Here we use a lattice Boltzmann model (LBM), to follow the evolution of flow streamlines in

a nanostructured MOF catalyst. By analyzing the flow patterns in different crystallographic directions, we show that there is a persistent anisotropy in the permeability of the MOF. Our findings show that such studies can be used to determine the role of the structure of the MOF in determining its permeability and possible interaction with a flowing analyte.

As a demonstration of the combined effect of gas flow and adsorption on the crystal lattice of a MOF, we performed in situ synchrotron powder X-ray diffraction (PXRD) measurements under gas-flow conditions. For this purpose, we chose the NU-1000, Zr-based MOF [$Zr_6(\mu_3-O)_4(\mu_3-OH)_4(OH)_4(H_2O)_4$(tbapy)$_2$; tbapy: tetratopic 1,3,6,8-tetrakis-(p-benzoate) pyrene].[20,21] NU-1000 is a nonisotropic framework with the pores arranged in two distinct channels, the larger one being 30 Å in size running along unit cell dimension *c* and the smaller ones ~9.8 Å in diameter,[22] running along *a* and *b* (Figure 1a). The gases were small molecules, namely, N_2 and CO_2, to better correspond to the theory and low Reynolds numbers. The PXRD data were collected at the beamline 17-BM of the Advanced Photon Source (APS) at Argonne National Laboratory. The data were analyzed with LeBail fit,[23] and corresponding unit-cell changes were extracted. Our results show that adsorption of both N_2 and CO_2 affects the unit cell of NU-1000, and the response is anisotropic. Upon gas adsorption we observed the expansion of the lattice dimension *c*, corresponding to the crystallographic [001] direction and contraction of lattice dimensions *a* ([100]) (Figure 1b) with the maximum change of ~0.25% expansion of *c* during the CO_2 adsorption at 200 K. The change is fully reversible upon the desorption of N_2/CO_2 in He. To model theoretically the time dependence of the structural changes in NU-1000 and other anisotropic MOFs, a new approach is required that takes into
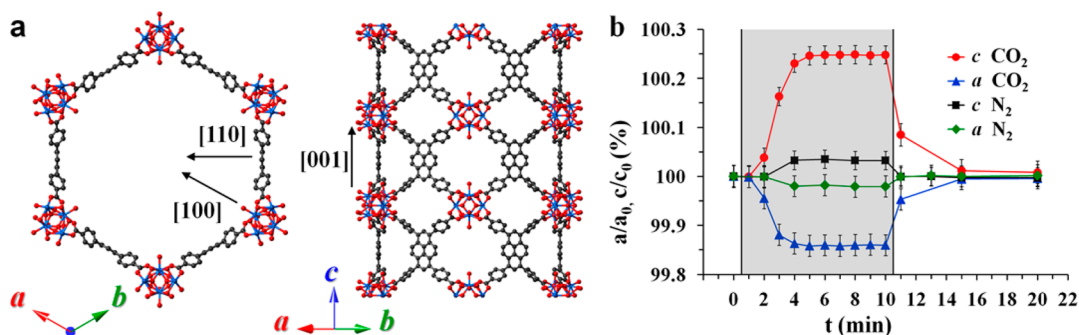
Figure 1. (a) Schematic of the NU-1000 structure. (b) Evolution of lattice parameters a and c during adsorption (gray area) and desorption of CO_2 and N_2 on NU-1000 at 200 K, as measured in the in situ PXRD experiment.

account the gas-flow direction within the MOF and its effect on permeability.

To model the permeability and its dependence on the transport direction, we used the LBM.[24] While the LBM has been extensively used to study fluid flow in porous media[25,26] in those cases the pore sizes were micron-scale or larger. Once pore sizes start approaching the nanoscale, the critical parameter that needs to be considered is the Knudsen number, which represents the ratio of the mean free path of the flowing gas relative to the pore size of the system. Previous studies using LBM to model flow through nanoporous membranes have shown that LBM can be used to simulate a range of Knudsen numbers by incorporating the appropriate boundary conditions at the pore-wall surface.[27] The choice of boundary conditions can be determined by calibrating the model to experiments. However, these studies also showed that for moderate Knudsen numbers the role of the nanoporous structure in modulating the flow showed qualitatively similar behavior regardless of the details of the boundary condition. In our simulations, we limited our studies to the low Knudsen number limit because we are interested in establishing a baseline for the interaction between the MOF and the flowing gas. In practical terms, this means that our studies are limited to small-molecule transport through the MOFs, and we can then use the LBM by invoking no momentum transfer between the nodes of the MOF and the gas.

The advantage of using the LBM is that it is a meshless approach and thus can be highly parallelized. Here space is discretized into regularly distributed nodes on a lattice and time is divided into evenly spaced intervals. Particle positions are confined to the nodes, and each node contains a particle population distribution in different directions that connects neighboring nodes.[24] In this limit, and invoking Bhatnagar, Gross, and Krook (BGK) dynamics,[28] the discrete lattice Boltzmann equation becomes

$$f_i(\boldsymbol{x} + \boldsymbol{e}_i \Delta t, t + \Delta t) = f_i(\boldsymbol{x}, t) - \frac{[f_i(\boldsymbol{x}, t - f_i^{\text{eq}}(\boldsymbol{x}, t))]}{\tau} \tag{1}$$

where $f_i(\boldsymbol{x}, t)$ is the local density distribution function in direction i and τ is the relaxation time. The equilibrium distribution function for the fluid is defined as

$$f_i^{\text{eq}} = \rho t_i \left[1 - \frac{\boldsymbol{u}^2}{2c_s^2} + \frac{\boldsymbol{u} \cdot \boldsymbol{e}_i}{c_s^2} + \frac{(\boldsymbol{u} \cdot \boldsymbol{e}_i)^2}{2c_s^4} \right] \tag{2}$$

where t_i is the weight constant in direction i and c_s is the speed of sound in the lattice. The macroscopic density ρ and velocity

$\boldsymbol{u}$ can be obtained by $\rho = \sum_i f_i$, and $\boldsymbol{u} = \frac{1}{\rho} \sum_i f_i \boldsymbol{e}_i$. Before performing the simulation we approximated the structure with a simple model, containing spheres with radii equal to the van der Waals radii[29] of the nodes and linkers (Supporting Information (SI), Figures S1 and S2). The details of the construction (Table S1) can be found in the SI. The first set of simulations was run to investigate the flow pattern through the NU-1000 structure. As shown in Figure 2, we calculated the
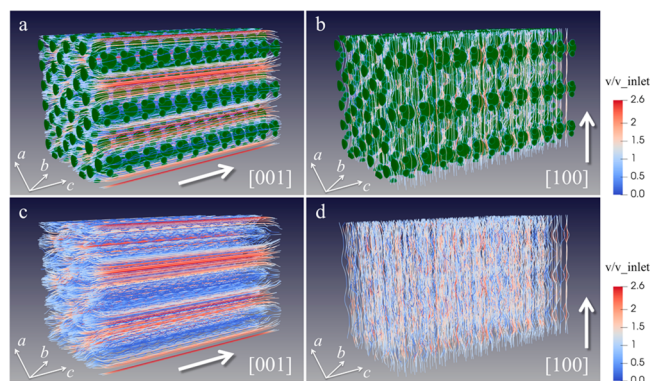
Figure 2. Streamlines for gas flow (a) parallel and (b) perpendicular to the channels in NU-1000, with green spheres for MOF nodes. The same streamlines are shown without MOF structure (c) parallel and (d) perpendicular to the channels. The local velocity was scaled by the inlet velocity to better visualize the disturbance of flow.

streamlines for the flow, for two cases, one in which the gas flow was parallel to the largest channels (direction [001]; see Figure 1) and the other when the flow was perpendicular to the channels (direction [100]). In this, and in all of the results presented, we scaled the local velocity by the inlet velocity to better visualize the disturbance of flow caused by the structure of the MOF. When the flow is parallel to the channels, we see large relative flow velocities along the channels as expected and low velocities elsewhere. When the flow is perpendicular to the channels, however, while we do see variations in the velocities, they appear not to be as severe as the previous case.
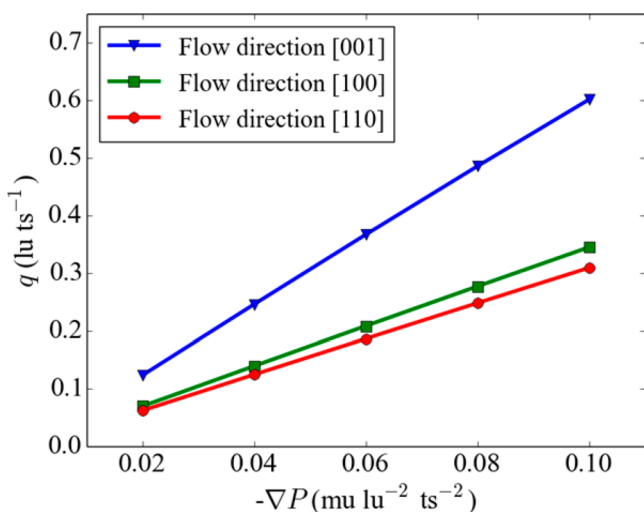
To further quantify the effect of the structural anisotropy of the NU-1000, we calculated velocity distributions using a cross section of the structure for both flow cases. The velocity distributions for different flow directions are compared in Figure 3. Figure 3a shows the distribution of velocities in [001] when the flow is parallel to the channels, while Figure 3b shows the distribution of velocities in [100] when the flow is perpendicular to the channels. Two points should be noted
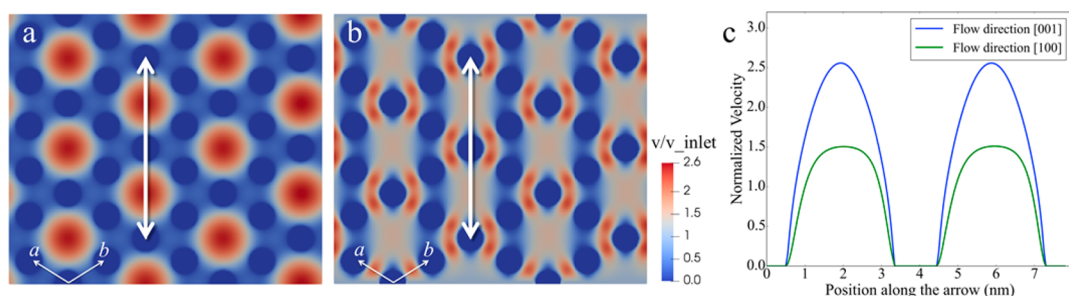
Figure 3. Velocity distributions for gas flow (a) parallel and (b) perpendicular to the channels in a cross section of NU-1000. The velocity distributions along the arrow for the two flow cases are compared in panel c. The local velocity was scaled by the inlet velocity to better visualize the disturbance of flow.

from this Figure: First, the variations in velocity are much larger in the case of [001] direction (Figure 3c). Second, if we assume that any component that is introduced along with the carrier gas will follow the streamlines, then there will be significantly more interaction with the MOF in [100].

While these studies show how the anisotropy of NU-1000 manifests itself in the flow streamlines, we still needed to see if this effect persists when we calculate transport properties, such as the permeability. So, for the next set of simulations we set up pressure gradients across the MOF and solved for the flux using the same two flow cases: parallel and perpendicular to the channels. According to Darcy's law,[30] if we plot the flux $q = -\frac{\kappa}{\mu}\nabla P$, where μ is the dynamic viscosity, against the negative pressure gradient $-\nabla P$, then the effective permeability κ should be proportional to the slope of the curve. As can be seen in Figure 4, there is a clear effect of the anisotropy of the

the positions of the atoms onto a single plane (Figure 5), when the flow is parallel to the channels, the area occupied by the

Figure 5. Projections of NU-1000 onto a single plane for flow (a) parallel, (b) perpendicular, and (c) perpendicular with 30° rotation along the large channel axis, where S is the percentage of the area occupied by the nodes.

nodes is 36% of the total area, whereas when the flow is perpendicular to the channels, the area occupied is 53%. The larger area occupied should therefore result in a lower permeability. However, while the geometry of the structure is important and does influence the flow pattern, there is not a one-to-one correspondence between the two. To demonstrate this, we ran a series of simulations in which we rotated the structure of NU-1000 about the long axis of the parallel channels such that the while orientation of the parallel channels was unchanged we now changed the structure perpendicular to the channels. For a 30° rotation, the projected occupied area increases to 85% for flow perpendicular to the channels. However, when we repeat the simulations using this rotated structure, we do not see a large change in the permeability (Figure 4). Thus our results cannot be explained by a simple geometric effect, and to fully understand the permeability of MOF structures, the detailed calculation of flow and residence times is needed.

The results validate our initial hypothesis that the anisotropy in the structure results in an anisotropic permeability of the material. Furthermore, the observed anisotropy is not entirely a result of a geometric effect and therefore cannot be simply explained by invoking the relative size of the channels in the different directions. Finally, we evaluate the relative change in permeability due to realistic (as observed in the experiment) changes in the lattice parameters of the MOF. Those changes were observed in the presence of CO_2 compared with the pristine MOF (Figure 1). The results are shown in Table S2, and, as can be seen, the permeability change qualitatively follows the structural change.

On the basis of our results we propose that the internal structure of the MOF, and its concomitant arrangement of pores, will strongly affect the flow dynamics of gas molecules
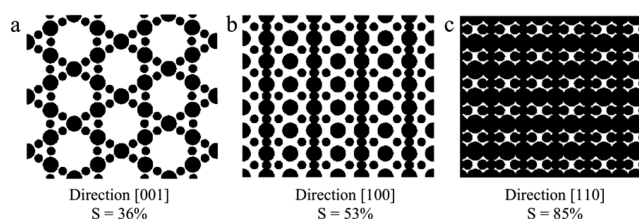

Figure 4. Flux versus negative pressure gradient for flow parallel to the channels (blue with triangle markers), perpendicular to the channels (green with square markers), and perpendicular to the channels with a 30° rotation about the long axis of the parallel channels (red with circle markers). In LBM, the units of mass, length, and time are mass unit (mu), lattice unit (lu), and time step (ts), respectively.

MOF structure on the permeability. The permeability when the flow is parallel to the channels in [001] is significantly higher than the permeability when the flow is perpendicular to the channels in [100].

At first glance, our results could be explained by a simple geometric effect. For example, if we make a projection of all of

and, as a result, the kinetics of adsorption. We expect that as we introduce larger molecules in the carrier gas, this effect could be magnified. This could have a significant impact on applications ranging from catalytic to sensing to filtration uses, where we could have, in principle, a broad residence time distribution of the adsorbents/reactants in the MOF resulting in possible inhomogeneities in the final product stream. Understanding the effect of the structure on the flow field and, consequently, reaction kinetics will allow us to engineer around possible bottlenecks and design MOFs with structures optimized for specific applications. For example, this approach will allow us to model possible pore blocking during transport and thus provide guidelines to the design of a new generation of MOF's, in which a gradient of porosity[31] can be engineered to mitigate pore-blocking effects. We also note that we plan to extend this model to study diffusive transport. Experimental studies on MOFs have shown that diffusion can be often separated into the two terms, one responsible for topology (that is the one that we are taking into account in our model) and the other for the interactions.[32] The diffusion can be written as $D = D_0 \exp\left(-\frac{E_a}{RT}\right)$, where E_a is the activation energy of diffusion and D_0 is the diffusion in the infinite temperature limit. Because our model can account for D_0, we can then also look at the effect of the structure on the diffusion of molecules. Finally, in future work, we plan to develop a hybrid LBM/Brownian Dynamics model in which the carrier gas hydrodynamics can be modeled by the LBM, and we can introduce larger molecules of interest via the Brownian Dynamics approach. This will allow us to add an addition level of complexity into the model, allowing us to better approximate real experimental conditions such as those measured in the in situ XRD experiments.

ASSOCIATED CONTENT

ⓢ Supporting Information

The Supporting Information is available free of charge on the ACS Publications website at DOI: 10.1021/acs.jpclett.8b00011.

> Details of the PXRD measurements, lattice Boltzmann simulations, illustration of the structure used in the LBM calculations, and the lists of simulation parameters. (PDF)

AUTHOR INFORMATION

Corresponding Authors
*E-mail: Anatoly.Frenkel@stonybrook.edu.
*E-mail: Dilip.Gersappe@stonybrook.edu.

ORCID ⓘ
Anna M. Plonka: 0000-0003-2606-0477
Anatoly I. Frenkel: 0000-0002-5451-1207

Notes
The authors declare no competing financial interest.

ACKNOWLEDGMENTS

REFERENCES

(1) Maurin, G.; Serre, C.; Cooper, A.; Férey, G. The new age of MOFs and of their porous-related solids. *Chem. Soc. Rev.* **2017**, *46* (11), 3104–3107.

(2) Rowsell, J. L.; Yaghi, O. M. Metal–organic frameworks: a new class of porous materials. *Microporous Mesoporous Mater.* **2004**, *73* (1), 3–14.

(3) Stock, N.; Biswas, S. Synthesis of metal-organic frameworks (MOFs): routes to various MOF topologies, morphologies, and composites. *Chem. Rev.* **2012**, *112* (2), 933–969.

(4) Liu, Y.; Howarth, A. J.; Vermeulen, N. A.; Moon, S.-Y.; Hupp, J. T.; Farha, O. K. Catalytic degradation of chemical warfare agents and their simulants by metal-organic frameworks. *Coord. Chem. Rev.* **2017**, *346*, 101–111.

(5) Yoon, M.; Srirambalaji, R.; Kim, K. Homochiral Metal–Organic Frameworks for Asymmetric Heterogeneous Catalysis. *Chem. Rev.* **2012**, *112* (2), 1196–1231.

(6) Kreno, L. E.; Leong, K.; Farha, O. K.; Allendorf, M.; Van Duyne, R. P.; Hupp, J. T. Metal–Organic Framework Materials as Chemical Sensors. *Chem. Rev.* **2012**, *112* (2), 1105–1125.

(7) Stassen, I.; Burtch, N.; Talin, A.; Falcaro, P.; Allendorf, M.; Ameloot, R. An updated roadmap for the integration of metal–organic frameworks with electronic devices and chemical sensors. *Chem. Soc. Rev.* **2017**, *46* (11), 3185–3241.

(8) Duan, J.; Jin, W.; Kitagawa, S. Water-resistant porous coordination polymers for gas separation. *Coord. Chem. Rev.* **2017**, *332*, 48–74.

(9) Peng, Y.; Li, Y.; Ban, Y.; Jin, H.; Jiao, W.; Liu, X.; Yang, W. Metal-organic framework nanosheets as building blocks for molecular sieving membranes. *Science* **2014**, *346* (6215), 1356–1359.

(10) Li, W.; Zhang, Y.; Zhang, C.; Meng, Q.; Xu, Z.; Su, P.; Li, Q.; Shen, C.; Fan, Z.; Qin, L.; Zhang, G. Transformation of metal-organic frameworks for molecular sieving membranes. *Nat. Commun.* **2016**, *7*, 11315.

(11) Furukawa, H.; Cordova, K. E.; O'Keeffe, M.; Yaghi, O. M. The Chemistry and Applications of Metal-Organic Frameworks. *Science* **2013**, *341* (6149), 1230444.

(12) Li, J.-R.; Sculley, J.; Zhou, H.-C. Metal–Organic Frameworks for Separations. *Chem. Rev.* **2012**, *112* (2), 869–932.

(13) Ren, J.; Dyosiba, X.; Musyoka, N. M.; Langmi, H. W.; Mathe, M.; Liao, S. Review on the current practices and efforts towards pilot-scale production of metal-organic frameworks (MOFs). *Coord. Chem. Rev.* **2017**, *352*, 187–219.

(14) López-Maya, E.; Montoro, C.; Rodríguez-Albelo, L. M.; Aznar Cervantes, S. D.; Lozano-Pérez, A. A.; Cenís, J. L.; Barea, E.; Navarro, J. A. R. Textile/Metal–Organic-Framework Composites as Self-Detoxifying Filters for Chemical-Warfare Agents. *Angew. Chem., Int. Ed.* **2015**, *54* (23), 6790–6794.

(15) Mondloch, J. E.; Katz, M. J.; Isley Iii, W. C.; Ghosh, P.; Liao, P.; Bury, W.; Wagner, G. W.; Hall, M. G.; DeCoste, J. B.; Peterson, G. W.; Snurr, R. Q.; Cramer, C. J.; Hupp, J. T.; Farha, O. K. Destruction of chemical warfare agents using metal–organic frameworks. *Nat. Mater.* **2015**, *14*, 512.

(16) Moon, S.-Y.; Liu, Y.; Hupp, J. T.; Farha, O. K. Instantaneous Hydrolysis of Nerve-Agent Simulants with a Six-Connected Zirconium-Based Metal–Organic Framework. *Angew. Chem., Int. Ed.* **2015**, *54* (23), 6795–6799.

(17) Gurdal, Y.; Keskin, S. Atomically Detailed Modeling of Metal Organic Frameworks for Adsorption, Diffusion, and Separation of Noble Gas Mixtures. *Ind. Eng. Chem. Res.* **2012**, *51* (21), 7373–7382.

(18) Skoulidas, A. I. Molecular Dynamics Simulations of Gas Diffusion in Metal–Organic Frameworks: Argon in CuBTC. *J. Am. Chem. Soc.* **2004**, *126* (5), 1356–1357.

(19) Liu, Y. J.; Meirer, F.; Krest, C. M.; Webb, S.; Weckhuysen, B. M. Relating structure and composition with accessibility of a single

catalyst particle using correlative 3-dimensional micro-spectroscopy. *Nat. Commun.* **2016**, *7*, 12634.

(20) Mondloch, J. E.; Bury, W.; Fairen-Jimenez, D.; Kwon, S.; DeMarco, E. J.; Weston, M. H.; Sarjeant, A. A.; Nguyen, S. T.; Stair, P. C.; Snurr, R. Q. Vapor-phase metalation by atomic layer deposition in a metal−organic framework. *J. Am. Chem. Soc.* **2013**, *135* (28), 10294−10297.

(21) Deria, P.; Mondloch, J. E.; Tylianakis, E.; Ghosh, P.; Bury, W.; Snurr, R. Q.; Hupp, J. T.; Farha, O. K. Perfluoroalkane functionalization of NU-1000 via solvent-assisted ligand incorporation: synthesis and CO2 adsorption studies. *J. Am. Chem. Soc.* **2013**, *135* (45), 16801−16804.

(22) Vandenbrande, S.; Verstraelen, T.; Gutiérrez-Sevillano, J. J.; Waroquier, M.; Van Speybroeck, V. Methane Adsorption in Zr-Based MOFs: Comparison and Critical Evaluation of Force Fields. *J. Phys. Chem. C* **2017**, *121* (45), 25309−25322.

(23) Le Bail, A. Whole powder pattern decomposition methods and applications: A retrospection. *Powder Diffr.* **2005**, *20* (4), 316−326.

(24) Thorne, D. T. *Lattice Boltzmann Modeling: An Introduction for Geoscientists and Engineers*; Springer: 2006.

(25) Ferréol, B.; Rothman, D. H. Lattice-Boltzmann simulations of flow through Fontainebleau sandstone. *Transp. Porous Media* **1995**, *20* (1), 3−20.

(26) Martys, N. S.; Chen, H. Simulation of multicomponent fluids in complex three-dimensional geometries by the lattice Boltzmann method. *Phys. Rev. E: Stat. Phys., Plasmas, Fluids, Relat. Interdiscip. Top.* **1996**, *53* (1), 743−750.

(27) Zhao, J.; Yao, J.; Zhang, M.; Zhang, L.; Yang, Y.; Sun, H.; An, S.; Li, A. Study of Gas Flow Characteristics in Tight Porous Media with a Microscale Lattice Boltzmann Model. *Sci. Rep.* **2016**, *6*, 32393.

(28) Bhatnagar, P. L.; Gross, E. P.; Krook, M. A model for collision processes in gases. I. Small amplitude processes in charged and neutral one-component systems. *Phys. Rev.* **1954**, *94* (3), 511.

(29) Bondi, A. van der Waals volumes and radii. *J. Phys. Chem.* **1964**, *68* (3), 441−451.

(30) Whitaker, S. Flow in porous media I: A theoretical derivation of Darcy's law. Transport in porous media. *Transp. Porous Media* **1986**, *1* (1), 3−25.

(31) Liu, C.; Zeng, C.; Luo, T.-Y.; Merg, A. D.; Jin, R.; Rosi, N. L. Establishing porosity gradients within metal−organic frameworks using partial postsynthetic ligand exchange. *J. Am. Chem. Soc.* **2016**, *138* (37), 12045−12048.

(32) Sharp, C. H.; Abelard, J.; Plonka, A. M.; Guo, W. W.; Hill, C. L.; Morris, J. R. Alkane-OH Hydrogen Bond Formation and Diffusion Energetics of n-Butane within UiO-66. *J. Phys. Chem. C* **2017**, *121* (16), 8902−8906.